frontiers | Frontiers in Chemistry

TYPE Original Research
PUBLISHED 27 February 2025
DOI 10.3389/fchem.2025.1544876

OPEN ACCESS

EDITED BY
Qinge Ma,
Jiangxi University of Traditional Chinese Medicine, China

REVIEWED BY
Bak Jia,
Kyungsung University, Republic of Korea
Batoul Izzularab,
Damanhour University, Egypt

*CORRESPONDENCE
Yunlong Xu,
16492111@qq.com
Huazhong Xiong,
xhz1004@163.com

RECEIVED 13 December 2024
ACCEPTED 16 January 2025
PUBLISHED 27 February 2025

CITATION
Wang Z, Xu Y and Xiong H (2025) Mechanism of salidroside promoting testosterone secretion induced by H_2O_2 in TM3 Leydig cells based on metabolomics and network pharmacology. *Front. Chem.* 13:1544876. doi: 10.3389/fchem.2025.1544876

Mechanism of salidroside promoting testosterone secretion induced by H_2O_2 in TM3 Leydig cells based on metabolomics and network pharmacology

Zixu Wang[1], Yunlong Xu[2]* and Huazhong Xiong[2]*

[1]College of Traditional Chinese Medicine, Changchun University of Chinese Medicine, Changchun, China, [2]Prevention and Treatment Center, Affiliated Hospital to Changchun University of Chinese Medicine, Changchun, China

Oxidative stress-induced damage is a significant contributor to the impairment of Leydig cells in the testes, potentially diminishing the secretion of testosterone and other androgens, thereby resulting in testosterone deficiency. Salidroside, the principal bioactive constituent derived from Rhodiola, exhibits potent antioxidant properties. This study aims to investigate the underlying mechanisms by which salidroside enhances testosterone secretion. The study investigated the oxidative damage in TM3 cells induced by H_2O_2 and demonstrated that salidroside significantly decreased the levels of ROS and MDA, while increasing the levels of testosterone, SOD, GSH. These changes effectively ameliorated oxidative stress, mitigated oxidative damage, protected TM3 cells, and enhanced testosterone secretion. Additionally, UPLC-QE-Orbitrap-MS was employed to analyze the metabolomics of TM3 cells, identifying 28 distinct metabolites and associated metabolic pathways. Key metabolic pathways identified include Arginine biosynthesis, Alanine, aspartate and glutamate metabolism, Citrate cycle (TCA cycle), Phenylalanine metabolism, Pyruvate metabolism. Utilizing network pharmacology, the core targets of salidroside in enhancing testosterone secretion were further investigated, revealing the involvement of AMACR, CYP3A4, ECHS1, HSD17B10, MPO, and TYR. This discovery was confirmed by dry-wet analysis. To sum up, salidroside can reduce the level of oxidative stress and promote testosterone secretion through multiple metabolic pathways and multiple targets. In a word, salidroside may provide a new strategy for preventing and treating testosterone deficiency.

KEYWORDS

salidroside, oxidative stress, testosterone, metabolomics, network pharmacology

1 Introduction

Testosterone (T) is the predominant androgen secreted in males, playing a crucial role in physiological functions. Inadequate secretion of testosterone can result in conditions such as erectile dysfunction, fatigue, and osteoporosis (Aversa and Morgentaler, 2015). Testicular interstitial cells, which are vital germ cells for sustaining normal reproductive physiology in male animals, are responsible for the synthesis and secretion of testosterone (Zhang et al., 2024). Research has demonstrated

that oxidative stress-induced injury is a critical factor contributing to the damage of Leydig cells in the testes, leading to a reduction in the secretion of testosterone and other androgens, thereby adversely affecting spermatogenesis (Zhang et al., 2022). Consequently, mitigating oxidative stress in compromised cells and safeguarding the functionality of oxidatively damaged Leydig cells are of paramount importance for enhancing testosterone production (Dalmasso et al., 2017). The exogenous testosterone supplement therapy not only has safety problems, but also may inhibit its own testosterone secretion after taking it for a long time. Therefore, it has become a hot research topic to find effective components from natural drugs that can promote endogenous testosterone synthesis.

Salidroside, a principal bioactive compound in the traditional Chinese medicinal herb Rhodiola, exhibits notable antioxidant (Zhu and Yu, 2024), anti-inflammatory (Rasmussen et al., 2024), anti-apoptotic (Gao et al., 2023), and anti-aging (Li M. et al., 2024) properties. Studies indicate that salidroside administration enhances erectile function in rats with bilateral cavernous nerve injury (Ye et al., 2021). This improvement is attributed to its capacity to inhibit cellular apoptosis and fibrosis through the promotion of protective autophagy, as well as its ability to ameliorate the depletion of neural components, endothelial cells, and smooth muscle cells within the cavernous body. Furthermore, a recent study indicates that salidroside may enhance the Nrf2/HO-1 signaling pathway and improve erectile function in diabetic male rats by mitigating oxidative stress and apoptosis in cavernous tissue (Li Z. et al., 2024). While the protective effects of salidroside in various diseases have been highlighted, its potential role in promoting testosterone secretion requires further elucidation through more comprehensive research. Therefore, it is urgent to further study the exact mechanism of salidroside promoting testosterone secretion by improving oxidative stress, so as to promote its subsequent development and utilization.

In recent years, metabolomics, along with other omics techniques, has been extensively utilized in biological research (Maniscalco et al., 2020). Metabolomics is a research methodology that emulates the investigative approaches of genomics and proteomics, facilitating the quantitative analysis of all metabolites within organisms and identifying correlations between these metabolites and physiological or pathological changes (Pognan et al., 2023). Moreover, network pharmacology research grounded in metabolomics can integrate clustering algorithms and network topology to investigate the interrelationships among components, targets, and metabolites, thereby enabling the elucidation of underlying biological network mechanisms.

In this study, the differential metabolites and related metabolic pathways of oxidative damage of salidroside on TM3 cells were analyzed by metabolomics. Combined with network pharmacology, the metabolic pathways of differential metabolites were annotated by genes, and the regulatory mechanism of salidroside in improving oxidative damage of Leydig cells was revealed from the perspective of genes and metabolites, which laid the foundation.

2 Materials and methods

2.1 Material

2.1.1 Materials and reagents

Salidroside was purchased from Shanghai Yuanye Technology Co., Ltd. (China, Shanghai), and the purity was over 98%. 30%H_2O_2 was purchased from Shanghai Macklin Biochemical Technology Co., Ltd. (China, Shanghai); DCFH-DA fluorescent probe was purchased from Beijing Solaibao Technology Co., Ltd. (China, Beijing). α-MEM medium, fetal bovine serum, penicillin (100 U/mL) and Streptomycin (100 μg/mL) were purchased from GIBCO Company. Testosterone, MDA, SOD and GSH kits were all purchased from Enzyme Immunity Biotechnology Co., Ltd. (China, Shanghai).

2.1.2 Experimental cells

Mouse Leydig cells TM3 were purchased from the cell bank of China Academy of Sciences (China, Shanghai).

2.2 Cell culture

TM3 cells were maintained in DMEM/F12 medium supplemented with 10% fetal bovine serum, 100 U/mL penicillin, and 100 μg/mL streptomycin, incubated at 37°C with 5% CO_2, and subcultured every 2–3 days.

2.3 Determination of TM3 cell viability by CCK-8 method

TM3 cells in the logarithmic growth phase were seeded into a 96-well plate at a concentration of 1×10^4 cells per well, cultured for 24 h, and then the culture medium was discarded. 200 μL salidroside (1,5,10,20,50,100 μM) with different concentrations was added and cultured for 24 h, or H_2O_2 (1,10,50,100,200,400 μM) with different concentrations was cultured for 1 h. After adding 10 μL of CCK-8 solution to each well, the absorbance was measured at 450 nm following a 1-h incubation. Cell viability (%) = ($OD_{\text{experimental groups}}$−$OD_{\text{blank groups}}$)/ ($OD_{\text{control groups}}$−$OD_{\text{blank groups}}$) ×100%.

2.4 Effect of salidroside on the viability of TM3 cells induced by H_2O_2

Based on the method in "2.3," they were grouped into control, H_2O_2-treated, and H_2O_2+Salidroside-treated group to investigate the impact of salidroside on the viability of TM3 cells induced by H_2O_2.

2.5 Detection of ROS content with DFCH-DA fluorescent probe

TM3 cells in logarithmic growth phase were inoculated in 6-well plates at a density of 1×10^6/well for 24 h. The cells were subjected to 100 μM H_2O_2 for 1 h and treated with drugs in groups for 24 h. They

were washed with PBS, stained with 10 μM DCFH-DA for 20 min in the dark, washed three times with PBS. ROS fluorescence probe DCFH-DA has excitation wavelength of 488 nm and emission wavelength of 525 nm, and the intracellular ROS level is detected by fluorescence microscope.

2.6 Enzyme-linked immunosorbent assay

Following the method in"2.3," they were categorized into control, H_2O_2-treated, and H_2O_2+Salidroside-treated group. The cell supernatant was gathered after 24 h of culture. Following the ELISA kit guidelines, the levels of testosterone, MDA, SOD, and GSH in the cell culture solution were measured.

2.7 Metabonomics analysis

2.7.1 Sample preparation of cell metabolomics

TM3 cells in logarithmic growth period were inoculated into culture bottles at a density of 1×10^7/well and cultured for 24 h. Divided into control group, model group and treated group. 100 μM H_2O_2 was induced for 1 h and treated for 24 h. Add precooled PBS solution and wash twice, collect cells, centrifuge and discard supernatant. Quick frozen in liquid nitrogen for 15 min and stored at −80°C. The cells were repeatedly frozen and crushed for 5 times, added with 1 mL of methanol: water = 4:1 solution, vortex for 30 s, and ultrasonically crushed in ice bath for 6 min. Centrifuge at 4°C, 13,000 r/min for 10 min. Used for UPLC-QE-Orbitrap-MS analysis, the supernatant was transferred to the injection vial. Quality control (QC) samples were prepared by mixing equal volumes of supernatant samples.

2.7.2 UPLC-QE-Orbitrap-MS analysis

AccucoreTMC18 column (2.1 × 100 mm, 1.7 μm). Mobile phase: 0.1% formic acid water (A) and acetonitrile (B), gradient elution: 0 ~ 4 min, 98% ~ 88% A; 4 ~ 10 min, 88%~76% A; 10–20 min, 76% ~ 0% A; 20–28 min, 0% A. Flow rate: 0.3 mL/min. Sample volume: 10 μL. Column temperature: 25°C.

Ion source: electrospray ion source (ESI); Detection mode: positive ion and negative ion detection mode; FullMS resolution: 70,000; Dd-MS resolution: 17,500; Scanning range: m/z 66.7 ~ 1,000; Atomizer temperature: 300°C; Drying gas temperature: 350°C; Capillary voltage: 3.5 kV; Breakage voltage: 220 V; Taper hole voltage: 65 V.

2.7.3 Data processing

The original data undergo processing with Compound Discoverer software, which includes peak identification, extraction, alignment, and integration. Following standardization, the data underwent analysis using multivariate statistical methods such as principal component analysis (PCA) and orthogonal partial least squares discriminant analysis (OPLS-DA). Using VIP>1 and $p < 0.05$ as criteria, differential metabolites were screened and identified through the HMDB (https://www.hmdb.ca) and METLIN (https://metlin.scripps.edu). MetaboAnalyst 5.0 software (http://www.MetaboAnalyst.ca/) facilitated the analysis of metabolic pathways for the screened differential metabolites.

2.8 Network pharmacological analysis

2.8.1 Analysis of the metabolic targets of diverse metabolites

The differential metabolites were input into the MetScape plug-in of Cytoscape 3.8.0 software to build a "differential metabolite-target" network.

2.8.2 Disease and salidroside target acquisition

Through PubChem (https://pubchem.ncbi.nlm.nih.gov/), SwissTargetPrediction (http://www.swisstargetprediction.ch/), SuperPred (https://prediction.charity.de/subpages/target _ prediction. Screening and predicting the disease targets of "testosterone deficiency" with the help of GeneCards (https://www.genecards.org/), OMIM (https://www.omim.org/) and TTD (https://db.idrblab.net/ttd/) databases.

2.8.3 PPI analysis

Identify salidroside, testosterone deficiency disorders, and metabolic targets, then use jvenn (https://jvenn.toulouse.inra.fr/app/example.html) to map interactive targets and determine the core targets. Targets related to the study were input into the String database (https://cn.string-db.org/cgi/input.pl) for analyzing protein-protein interactions, and visual analysis was conducted with Cytoscape 3.10.1 software.

2.8.4 GO and KEGG analysis

The associated targets were entered into the Metascape database (https://metascape.org/gp/index.html#/main/step1) for enrichment analysis of GO and KEGG pathways, using a significance threshold of $p < 0.05$. The results were subsequently visualized utilizing the micro-information platform.

2.8.5 Construction of "drug-metabolite-target-pathway-disease" network

The study identified signal pathways associated with testicular deficiency and sorted the genes in the top 20 pathways according to their P values. Finally, the drug-metabolite-target-pathway-disease network was constructed by Cytoscape 3.8.0 software.

2.9 Molecular docking

AutoDock Vina 1.2.2 was used to dock ligand components with receptor protein molecules, and the stability of ligand-receptor binding was analyzed according to the calculated binding energy. The binding mode of receptor and ligand was visualized by Discovery Studio 2019, which showed that ligand receptor was bound by hydrogen bonds and amino acid residues.

2.10 Molecular dynamics simulation

Utilizing the molecular docking results as the initial configuration, the system was simulated using Gromacs2022.2 software. The CHARMM36 force field was employed, and the TIP3P model was chosen for water representation. The system underwent solvation and ion equilibration processes. Subsequently, the canonical ensemble

TABLE 1 RT-qPCR analysis of gene and associated basesequences.

GeneName	Forward (5′-3′)	Reverse (5′-3′)
GAPDH	CCTCGTCCCGTAGACAAAATG	TGAGGTCAATGAAGGGGTCGT
CYP3A4	TGCCTGCTCTTACTGGCTGGAG	TGGGTCTGGCTGACTGGGAAG
HSD17B10	GCATCCAAAGGGGGCATAGT	CTGGCCAAGAAGTTTCGCAC
MPO	CAGTAGACCCTCGAATCGCC	GGGCCGGTACTGATTGTTCA
TYR	ACACACTGGAAGTATTTTTGAACA	TAGGTGCATTGGCTTCTGGG
AMACR	TCACGATCCAACGAAAGGCT	GCAGAAAGCTGCCACAAGTT
ECHS1	TGGGGATAAGGCCTTTGCAG	TGCGATGACCGGTTTCTTGA

(NVT) and isothermal-isobaric ensemble (NPT) were applied to equilibrate the system, followed by conducting molecular dynamics simulations under standard temperature and pressure conditions. Following the molecular dynamics calculation, the structural features of the molecular dynamics trajectories were analyzed using root mean square deviation (RMSD), root mean square fluctuation (RMSF), gyration radius (RG), and the number of hydrogen bonds.

2.11 Detection of testosterone secretion related genes by RT-qPCR

TM3 cells were cultured at a density of 2×10^3 cells per well and allocated into three groups: control, model, and salidroside treated. Following a 24 h treatment period, the cells were harvested for analysis. The total RNA was extracted by TRIzol method, and the cDNA was synthesized by reverse transcription with PrimeScript™ RT reagent Kit with gDNA Eraser (Perfect Real Time) kit. Real-time fluorescence quantitative PCR analysis was performed by TB Green® Premix Ex Taq™ (Tli RNaseH Plus) kit to detect the expression of related genes. Using Primer-Blast tool of NCBI (https://www.ncbi.nlm.nih.gov/) database to query the mRNA sequence of target gene for primer design. Primer sequences are detailed in Table 1. GAPDH served as the internal reference gene for normalization, and the relative expression levels were calculated using the $2^{-\Delta\Delta CT}$ method.

2.12 Statistical analysis

All experiments should be repeated at least three times, and the values are expressed in mean ± SD. GraphPadPrism 8 software was used for statistical analysis. The statistical significance was determined by t-test or one-way analysis of variance (ANOVA). Among them, $p < 0.05$ was statistically significant.

3 Results

3.1 Effect of salidroside on oxidative damage of TM3 cells

As shown in Figure 1A, when the concentration of salidroside reached 100 μM, the cell viability decreased slightly. Therefore, 1, 5, 10, 20 and 50 μM were selected as the experimental concentrations for the following experiments. Figure 1B illustrates the induction of TM3 cells by varying concentrations of H_2O_2 over a 1 h period. It was observed that at H_2O_2 concentrations below 100 μM, the cell survival rate exceeded 50%. Conversely, when the concentration surpassed 200 μM, the cell survival rate fell below 50%, rendering it unsuitable for subsequent experimental operation. Consequently, a concentration of 100 μM H_2O_2 was selected to induce oxidative damage in TM3 cells. As depicted in Figure 1C, there was a statistically significant reduction in cell viability in the model group compared to the control group ($p < 0.05$). Compared with the model group, the cell viability of salidroside with different concentrations increased significantly ($p < 0.05$, $p < 0.01$). The result of ROS content is shown in Figure 1D. Compared with the control group, the relative content of ROS in TM3 cells in the model group increased ($p < 0.01$). Compared with the model group, the relative content of reactive oxygen species in salidroside group decreased ($p < 0.05$, $p < 0.01$).

3.2 Effects of salidroside on the contents of testosterone, SOD, MDA and GSH in TM3 cells

As shown in Figures 2A–D, the contents of testosterone, MDA, SOD and GSH in the cells of each group were compared, and the differences were statistically significant by analysis of variance ($p < 0.05$, $p < 0.01$). Compared with the control group, the level of MDA in TM3 cells in the model group increased, while the levels of testosterone, SOD and GSH decreased. Compared with the model group, the level of MDA in the salidroside group decreased, while the levels of testosterone, SOD and GSH increased in a concentration-dependent manner.

3.3 Metabolomics analysis

3.3.1 Metabolomics QC sample detection

QC samples are evaluated during the analysis process to ensure the stability and reliability of the system and data. Then, all samples were analyzed by PCA. As can be seen in Figure 3, the QC samples show good clustering in the PCA score graph, demonstrating system and data stability.

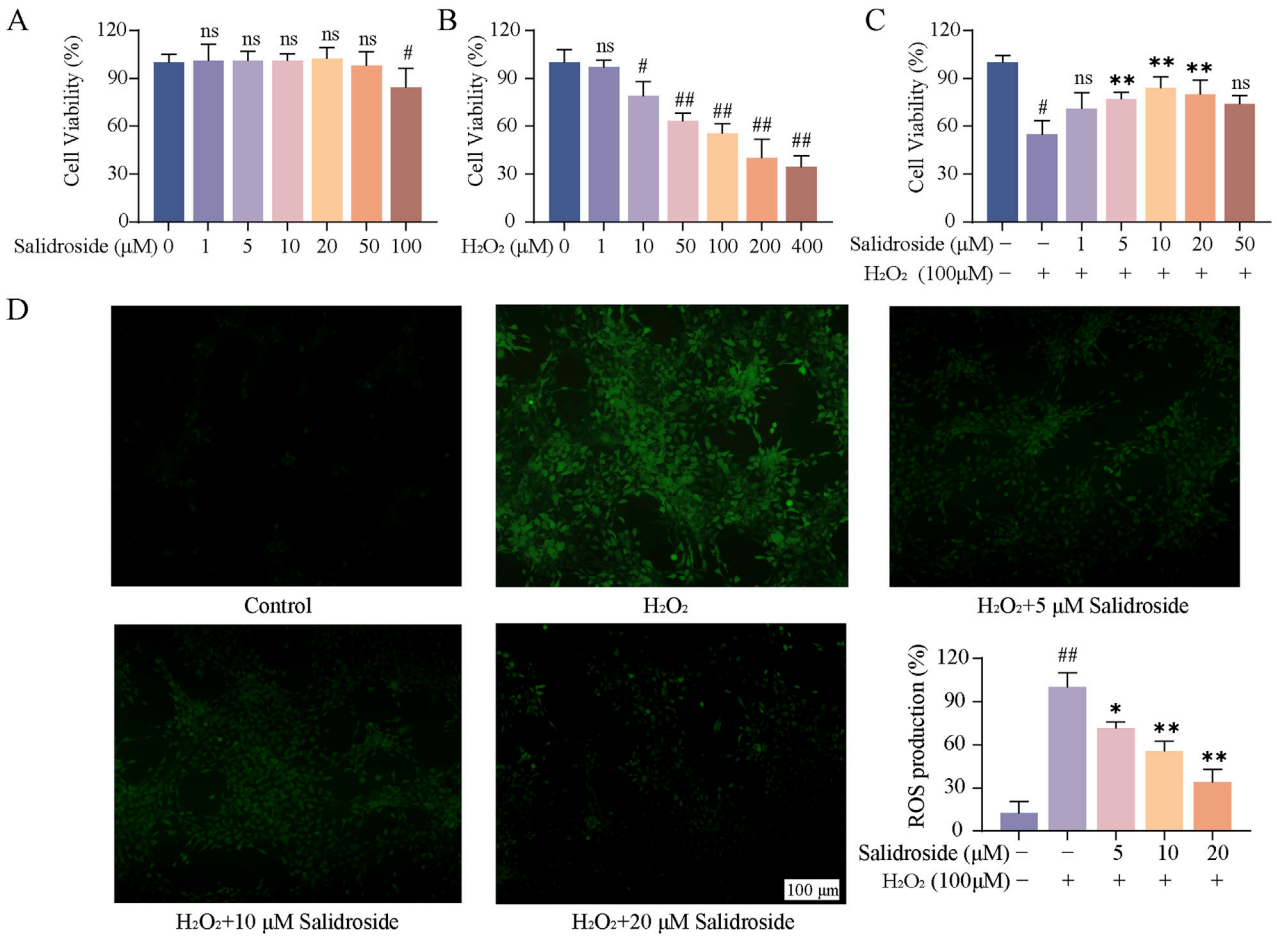

FIGURE 1
Effect of salidroside on oxidative damage of TM3 cells. **(A)** The effect of salidroside on the viability of TM3 cells. **(B)** Effect of H_2O_2 on the viability of TM3 cells. **(C)** Effect of salidroside on the viability of TM3 cells induced by H_2O_2. **(D)** The effect of salidroside on H_2O_2-induced ROS in TM3 cells. (mean ± SD, n = 3). Compared with the control group, $^{\#}p < 0.05$, $^{\#\#}p < 0.01$; Compared with the model group, $^{*}p < 0.05$, $^{**}p < 0.01$; Ns indicates that there is no significant difference.

3.3.2 Multivariate statistical analysis

As can be seen from Figure 3, the metabolic components of the three groups showed a partial separation trend, especially in the blank group and the model group, which showed that H_2O_2-induced TM3 cells caused differences in cell metabolites. In order to further screen the differences between groups, OPLS-DA was used to further analyze the cell metabolism samples. OPLS-DA score shows that the control group and the model group are obviously separated (positive ion mode $R^2X = 0.303$, $R^2Y = 0.999$, $Q^2 = 0.873$; The negative ion mode $R^2X = 0.343$,$R^2Y = 0.991$, $Q^2 = 0.791$). After salidroside treated, the model group and salidroside group were obviously separated, indicating that the metabolites in TM3 cells changed significantly after salidroside intervention (positive ion mode $R^2X = 0.229$, $R^2Y = 0.997$, $Q^2 = 0.746$; The negative ion mode $R^2X = 0.309$, $R^2Y = 0.992$, $Q^2 = 0.785$), as shown in Figure 4. Moreover, the regression lines of Q2 in both positive and negative ion modes intersect the negative semi-axis of *Y*-axis, which shows that the model has good stability, no over-fitting, and good prediction ability and reliability.

3.3.3 Differential metabolite analysis

According to OPLS-DA model, with VIP>1 and $p < 0.05$ as the standard, the different metabolites between groups were screened. The potential biomarkers were compared by Mtelin, HMDB and other metabolite databases, and 28 different metabolites were identified in positive and negative ion modes. See Figure 5A; Table 2.

3.3.4 Metabolic pathway analysis of differential metabolites

By using MetaboAnalyst 5.0, the metabolic pathway topology analysis and enrichment analysis of the differential metabolites were carried out, and the following metabolic pathways were selected as the key related metabolic pathways, as shown in Figure 5C. The results showed that salidroside mainly affected metabolic pathways such as Arginine biosynthesis, Alanine, aspartate and glutamate metabolism, Citrate cycle (TCA cycle), Phenylalanine metabolism and Pyruvate metabolism. Furthermore, the metabolic pathway of salidroside affecting testosterone secretion in TM3 cells was constructed through metabolic pathway (As shown in Figure 6).

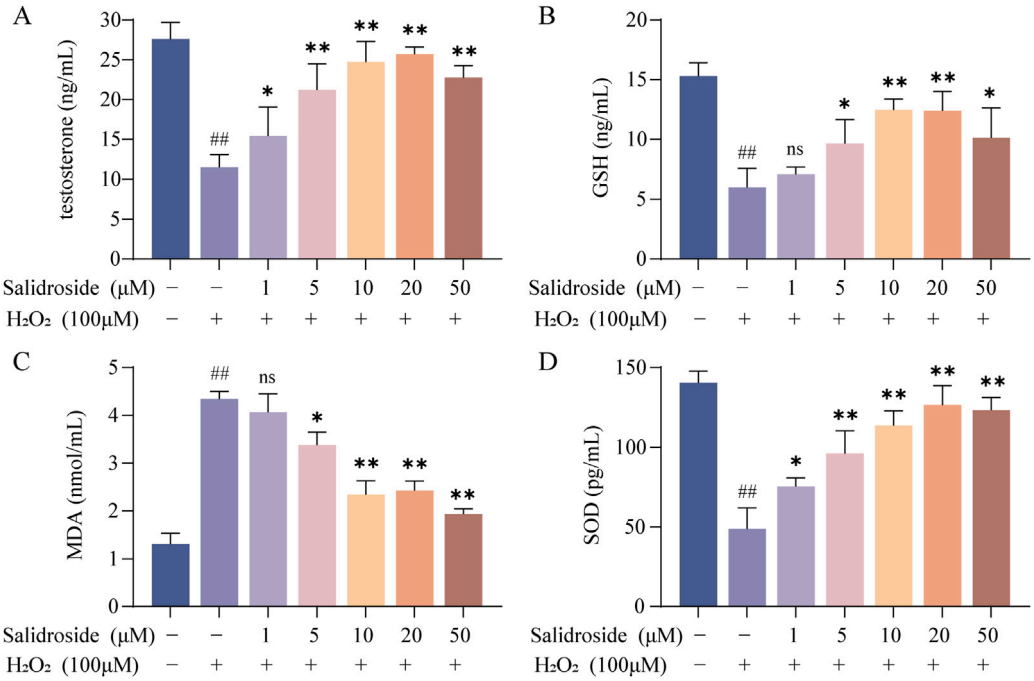

FIGURE 2
The contents of testosterone, SOD, MDA and GSH were detected by ELISA. **(A–D)** The effect of salidroside on the contents of testosterone, SOD, MDA and GSH in TM3 cells. (mean ± SD, n = 3). Compared with the control group, $^{\#\#}p < 0.01$; Compared with the model group, $^{*}p < 0.05$, $^{**}p < 0.01$; Ns indicates that there is no significant difference.

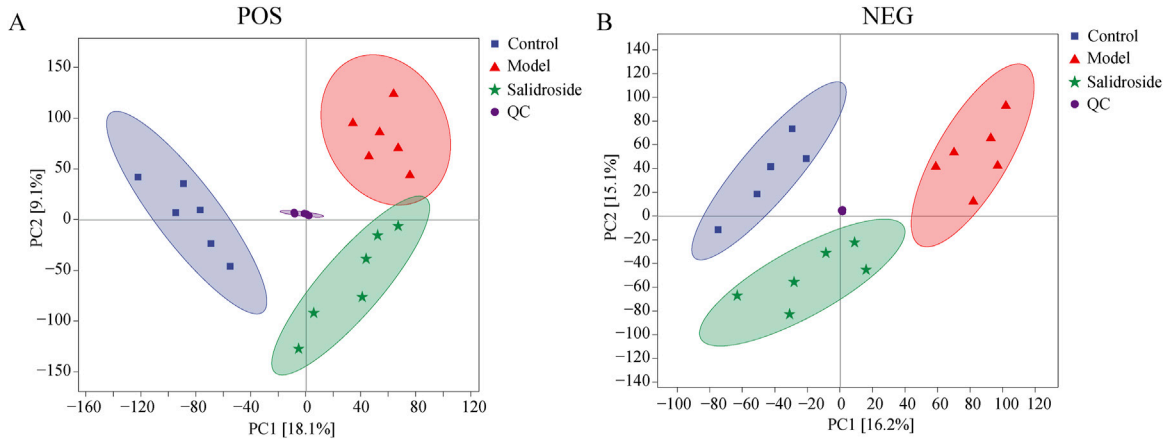

FIGURE 3
Score plots of QC, Sham, Model and salidroside groups in POS **(A)** and NEG mode **(B)**.

3.4 Network pharmacological analysis

3.4.1 Analysis of metabolic targets of differential metabolites

The metabolic targets of different metabolites were analyzed based on Cytoscape 3.8.0 software, and 312 metabolic targets were obtained, as shown in Figure 7A.

3.4.2 Acquisition of metabolic target, salidroside and common targets of disease

Salidroside and testosterone deficiency predicted 199 and 597 related targets respectively. A total of six common targets were obtained by cross-mapping with metabolic targets as potential targets for further research. As shown in Figures 7B, C.

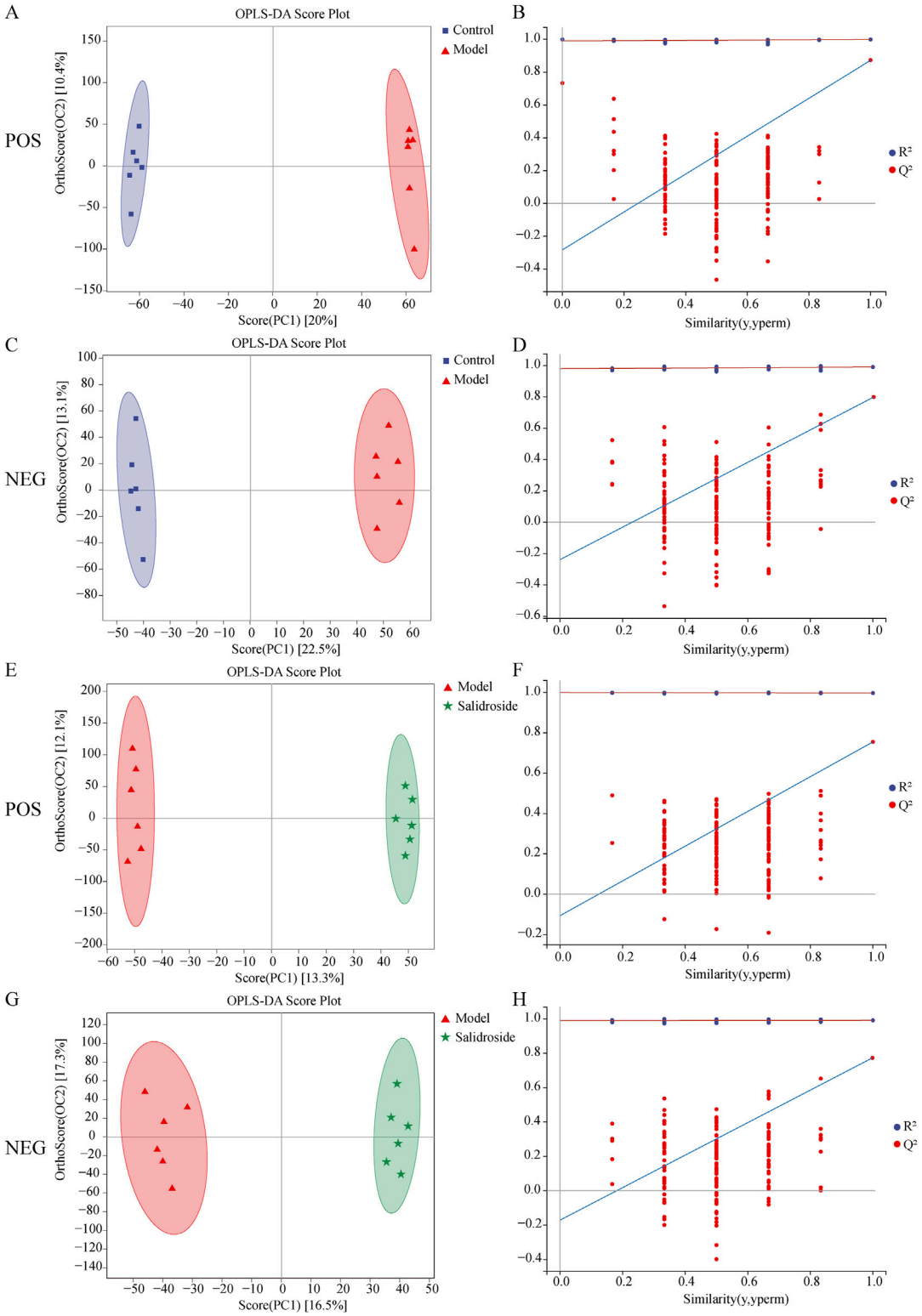

FIGURE 4
Results of OPLS-DA model in positive mode **(A)** and negative mode **(C)** using control and model group data and results of OPLS-DA model in positive mode **(E)** and negative mode **(G)** using model group and salidroside group data. Permutations Plot analysis **(B, D, F, H)**. The Q^2 regression line's intersection with the Y-axis was less than zero, showing that the model was valid.

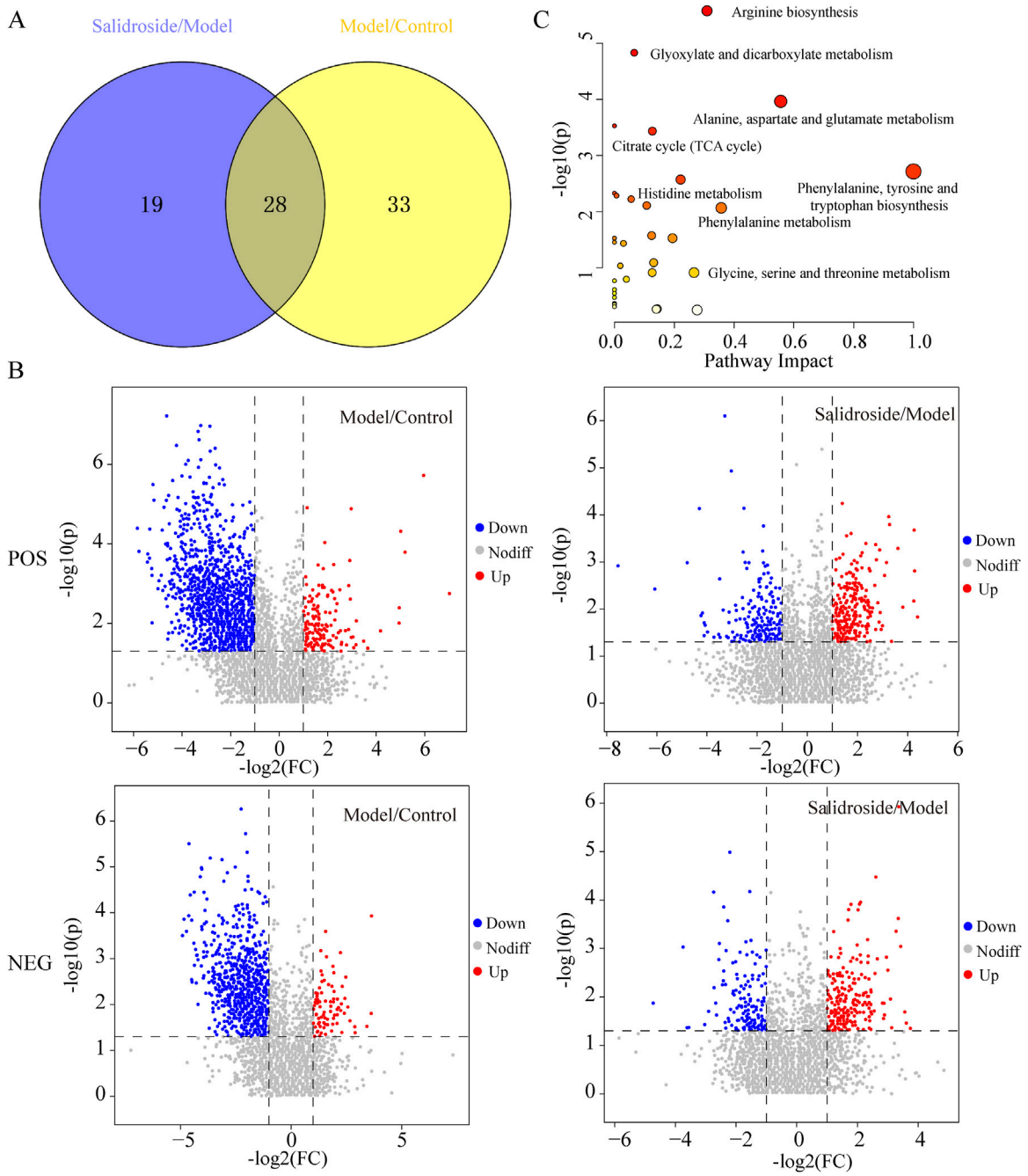

FIGURE 5
Differential metabolite analysis. **(A)** Venn diagram of differential metabolite. **(B)** Volcanic maps of Model/Control and Salidroside/Model in positive and negative ion mode. **(C)** Enrichment analysis of differential metabolite pathways.

3.4.3 GO and KEGG analysis

In order to further clarify the biological process related to the core target, GO and KEGG enrichment analysis were carried out (As shown in Figures 8A–D). GO analysis mainly involves carboxylic acid metabolism, amino acid metabolism, oxidoreductase activity and steroid hydroxylase activity. KEGG enrichment analysis mainly involves amino acid biosynthesis, steroid hormone biosynthesis, glycolysis/gluconeogenesis, arginine biosynthesis and other signal pathways. Construct "component-target-pathway-disease" network, as shown in Figure 8E.

3.5 Molecular docking

Molecular docking was used to evaluate the affinity between salidroside and the core target. It is generally believed that the lower the binding energy, the better the docking effect, indicating that the more stable the binding between active component ligand molecules and core target receptor proteins, the higher the affinity. The binding energies of the compounds were calculated by AutoDock Vina software. The results showed that the binding energies were lower than −5 kcal/mol and the compounds had good affinity.

10.3389/fchem.2025.1544876

TABLE 2 Differential metabolite analysis.

NO.	Rt (min)	m/z	Metabolites	Ion	Formula	HMDB	Model/Control	Salidroside/Model
1	0.53	147.1122	L-Lysine	$[M + H]^+$	$C_6H_{14}N_2O_2$	HMDB0000182	↓**	↑**
2	0.65	132.0761	creatine	$[M + H]^+$	$C_4H_9N_3O_2$	HMDB0000064	↓*	↑*
3	0.74	123.0557	Niacinamide	$[M + H]^+$	$C_6H_6N_2O$	HMDB0001406	↓*	↑**
4	0.86	182.0807	L-tyrosine	$[M + H]^+$	$C_9H_{11}NO_3$	HMDB0000158	↓*	↑**
5	0.95	243.0615	Uridine	$[M-H]^-$	$C_9H_{12}N_2O_6$	HMDB0000296	↓*	↑*
11	0.97	268.1029	Adenosine	$[M + H]^+$	$C_{10}H_{13}N_5O_4$	HMDB0000050	↓*	↑**
6	1.03	608.0886	UDP-N-acetylglucosamine	$[M + H]^+$	$C_{17}H_{27}N_3O_{17}P_2$	HMDB0000290	↓**	↑*
7	1.25	106.0499	Serine	$[M + H]^+$	$C_3H_7NO_3$	HMDB0003406	↓*	↑*
8	1.45	269.0874	Inosine	$[M + H]^+$	$C_{10}H_{12}N_4O_5$	HMDB0000195	↓*	↑*
9	1.68	150.0588	L-Methionine	$[M + H]^+$	$C_5H_{11}NO_2S$	HMDB0000696	↓**	↑**
10	2.87	229.1539	Leucylproline	$[M + H]^+$	$C_{11}H_{20}N_2O_3$	HMDB0011175	↓*	↑*
12	3.42	130.086	Leucine	[M−H]−	$C_6H_{13}NO_2$	HMDB0000687	↓*	↑*
13	3.58	175.1182	L-Arginine	$[M + H]^+$	$C_6H_{14}N_4O_2$	HMDB0000517	↓**	↑*
14	3.83	166.0867	L-Phenylalanine	$[M + H]^+$	$C_9H_{11}NO_2$	HMDB0000159	↑*	↓*
15	5.76	220.1183	Pantothenic acid	$[M + H]^+$	$C_9H_{17}NO_5$	HMDB0000210	↑*	↓*
16	5.94	148.0607	L-Glutamic acid	$[M + H]^+$	$C_5H_9NO_4$	HMDB0000148	↓*	↑*
17	6.53	247.1279	Glutamylvaline	$[M + H]^+$	$C_{10}H_{18}N_2O_5$	HMDB0028832	↓*	↑*
18	6.59	291.1302	Argininosuccinic acid	$[M + H]^+$	$C_{10}H_{18}N_4O_6$	HMDB0000052	↓*	↑**
19	8.76	133.0135	L-Malic acid	$[M - H]^-$	$C_4H_6O_5$	HMDB0000156	↓*	↑**
20	9.58	119.0337	Succinic acid	$[M + H]^+$	$C_4H_6O_4$	HMDB0000254	↓*	↑*
21	9.71	137.0452	Hypoxanthine	$[M + H]^+$	$C_5H_4N_4O$	HMDB0000157	↓**	↑*
22	10.32	203.2233	Spermine	$[M + H]^+$	$C_{10}H_{26}N_4$	HMDB0001256	↓*	↑*
23	14.72	134.0445	L-Aspartic acid	$[M + H]^+$	$C_4H_7NO_4$	HMDB0000191	↓*	↑**
24	15.19	145.0611	L-Glutamine	$[M-H]^-$	$C_5H_{10}N_2O_3$	HMDB0000641	↓*	↑*
25	16.67	151.0253	Xanthine	$[M-H]^-$	$C_5H_4N_4O_2$	HMDB0000292	↑*	↓*
26	17.53	166.9742	Phosphoenolpyruvic acid	$[M-H]^-$	$C_3H_5O_6P$	HMDB0000263	↓*	↑**
27	18.41	175.0241	cis-Aconitic acid	$[M + H]^+$	$C_6H_6O_6$	HMDB0000072	↓*	↑*
28	21.24	303.2315	Arachidonic acid	$[M-H]^-$	$C_{20}H_{32}O_2$	HMDB0001043	↓**	↑*

Finally, the visual analysis was performed with the Discovery Studio 2019 software, as shown in Figure 9.

3.6 Molecular dynamics simulation

Through metabolomics combined with network pharmacological analysis and molecular docking results, the core targets AMACR, CYP3A4, ECHS1, HSD17B10, MPO, TYR and salidroside were selected for molecular dynamics simulation verification. RMSD value is used to evaluate whether the simulation system reaches a stable state, and the RMSD value within 1 nm indicates the relative stability of protein-ligand interaction in physiological environment, and the results are shown in Figure 10A. To analyze the Molecular dynamics of the residues of various proteins in the complex during the simulation process, the RMSF values of all protein residues during the simulation process were calculated, the greater the interaction between the residues of the protein and the small molecule, see Figure 10B. RG represents the compactness of protein structure in the simulation process, as shown in Figure 10C, and salidroside is closely bound to each target. Hydrogen bonding is one of the strongest noncovalent interactions in the binding process between small molecular compounds and proteins. The number of hydrogen bonds reflects the strength of protein-ligand binding. As shown in Figure 10D, hydrogen bonding plays an important role in the stable existence of six complexes. Results It was verified that all targets and corresponding compounds could bind stably.

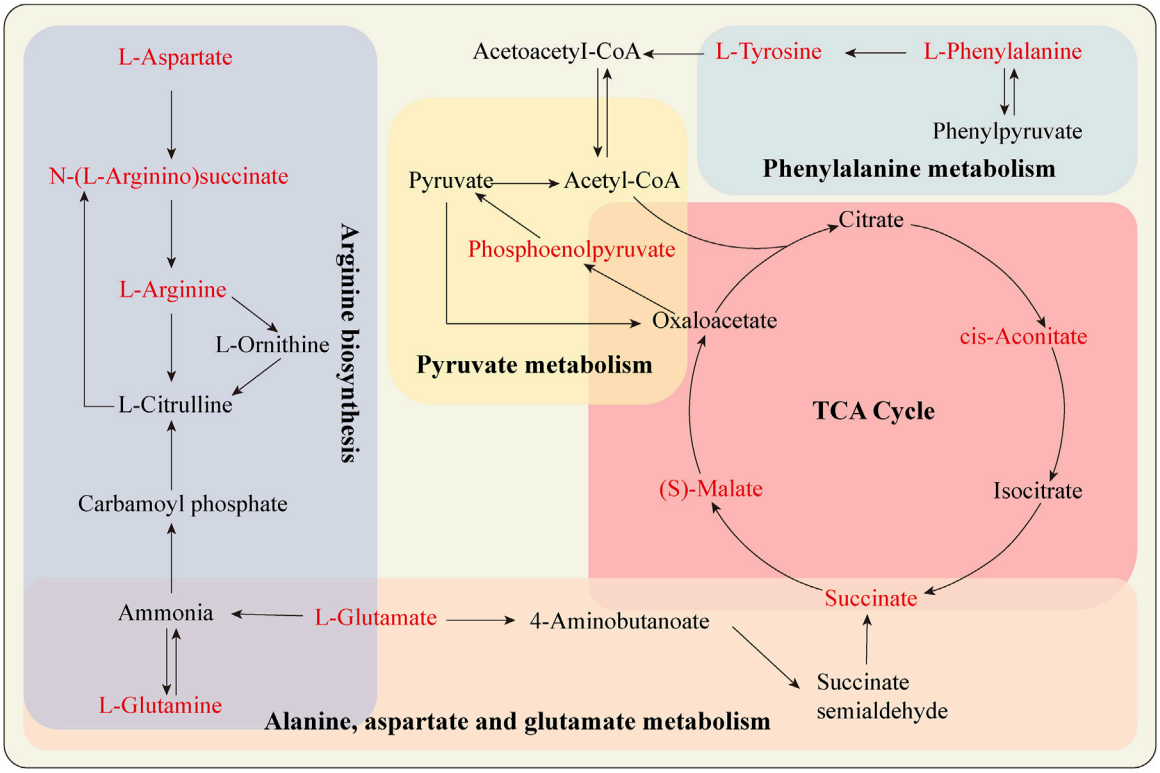

FIGURE 6
Analysis of metabolic pathways of differential metabolites.

3.7 RT-qPCR analysis

As shown in Figure 11. RT-qPCR results showed that the core targets were AMACR, CYP3A4, ECHS1, HSD17B10, MPO and TYR. Compared with the control group, the levels of AMACR, ECHS1, HSD17B10, MPO and TYR in the model group decreased significantly ($p < 0.05$, $p < 0.01$), while the levels of CYP3A4 increased ($p < 0.01$). Compared with the model group, the expressions of AMACR, ECHS1, HSD17B10, MPO and TYR in salidroside treated group increased significantly ($p < 0.05$, $p < 0.01$), while the expression of CYP3A4 decreased ($p < 0.05$, $p < 0.01$). It further shows that salidroside can promote testosterone secretion through the above six core targets.

4 Discussion

The testicles are critical reproductive organs in male animals, primarily responsible for the secretion of androgens, with testosterone being a principal hormone. Testosterone synthesis involves a series of enzymatic reactions and is predominantly secreted by the Leydig cells within the testes (Nassar and Leslie, 2023). A deficiency in testosterone can lead to conditions such as sexual dysfunction and metabolic disorders. Conversely, enhanced testosterone secretion has been shown to ameliorate hypogonadism (Groti Antonič and Zitzmann, 2024), improve glycemic control in diabetes (Ashour, 2024), treat atherosclerosis in middle-aged and elderly individuals (Albuquerque et al., 2020), and address osteoporosis (Mbiydzenyuy and Qulu, 2024). Research has indicated that oxidative stress-induced damage to Leydig cells in the testes is a significant contributor to male infertility. In this study, we developed an oxidative damage model of TM3 cells using H_2O_2 and discovered that salidroside enhances TM3 cell activity. This enhancement is evidenced by a significant increase in testosterone, SOD, and GSH levels, alongside a reduction in ROS and MDA levels. It shows that salidroside can effectively improve oxidative stress, reduce oxidative damage, protect TM3 cells and promote testosterone secretion.

It is worth noting, but there is no exact mechanism that salidroside promotes testosterone secretion by improving oxidative stress. Metabolomics serves as a tool to investigate the internal alterations within organisms, with metabolites representing the ultimate products of gene transcription and the foundational material basis of organismal phenotypes (Wishart, 2019). In this study, cell metabolomics was employed to delineate the metabolic pathway modulated by salidroside, as inferred from the downstream small molecular differential metabolites. Salidroside has been identified to influence the production of 28 distinct metabolites, such as arginine, aspartic acid, leucine, and arachidonic acid, among others. These metabolites are primarily associated with metabolic pathways including arginine biosynthesis, alanine, aspartate, and glutamate metabolism, the citrate cycle (TCA cycle), phenylalanine metabolism, and pyruvate metabolism. These findings demonstrate that salidroside plays a role in multiple metabolic pathways, contributing to the regulation of testosterone secretion.

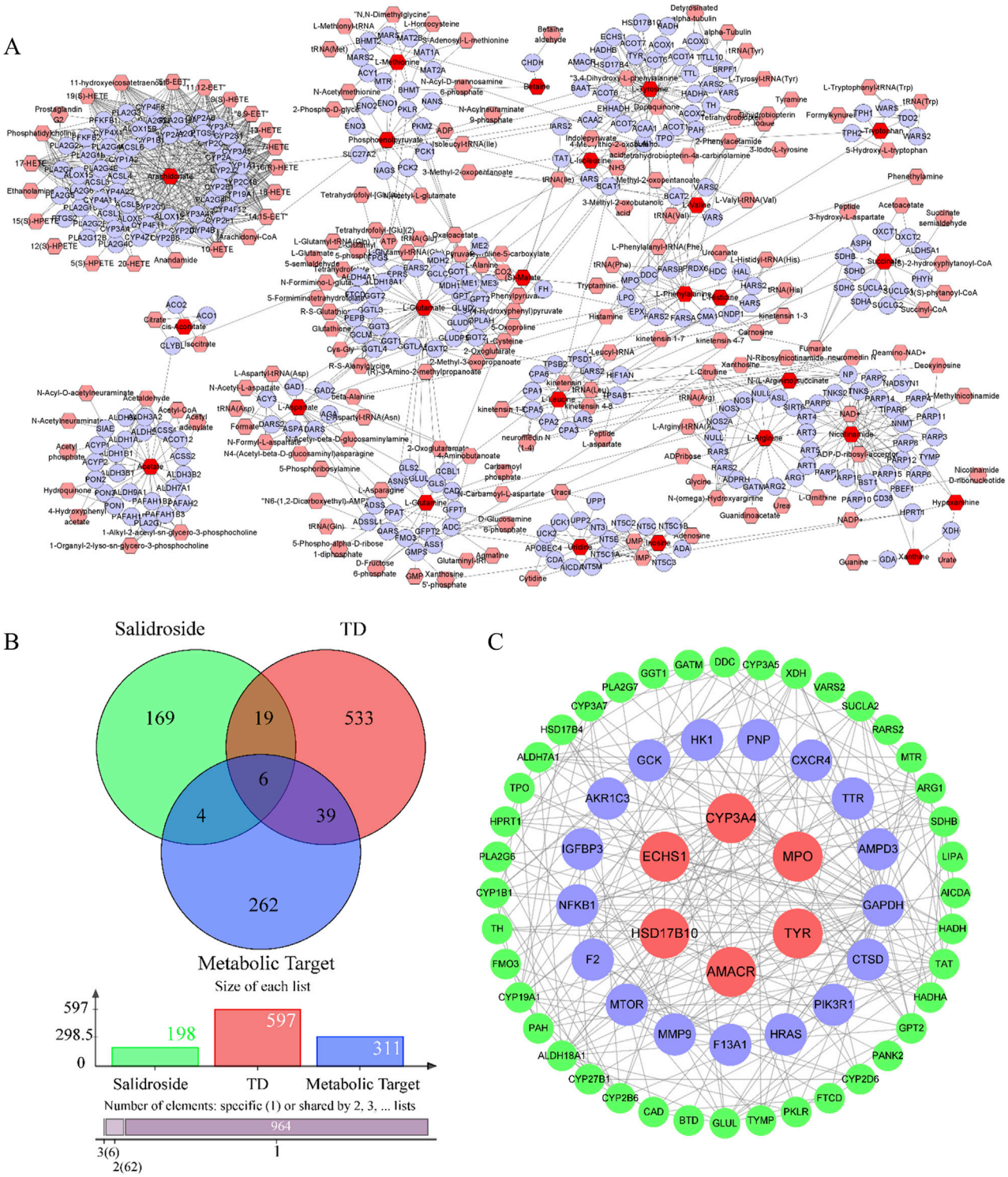

FIGURE 7
Analysis of network pharmacology. **(A)** Metabolic targets of differential metabolites. **(B)** Intersecting targets. **(C)** PPI network.

Interestingly, arginine biosynthesis is very important for epididymal sperm maturation (Tsuchiya et al., 2023; Wu et al., 2024). L-arginine, a precursor of nitric oxide, is essential for maintaining normal cellular nitric oxide levels (Wu et al., 2021). Nitric oxide is implicated in the regulation of mitochondrial biogenesis, the respiratory chain, and oxidative stress. In the testes, D-aspartic acid has been shown to enhance testosterone release, upregulate androgen receptor expression, and downregulate estrogen receptor expression (Roshanzamir and Safavi, 2017; Falvo et al., 2024). Furthermore, tyrosine and phenylalanine serve as precursors in the biosynthesis of neurotransmitters and hormones (Schenck and Maeda, 2018; Lu

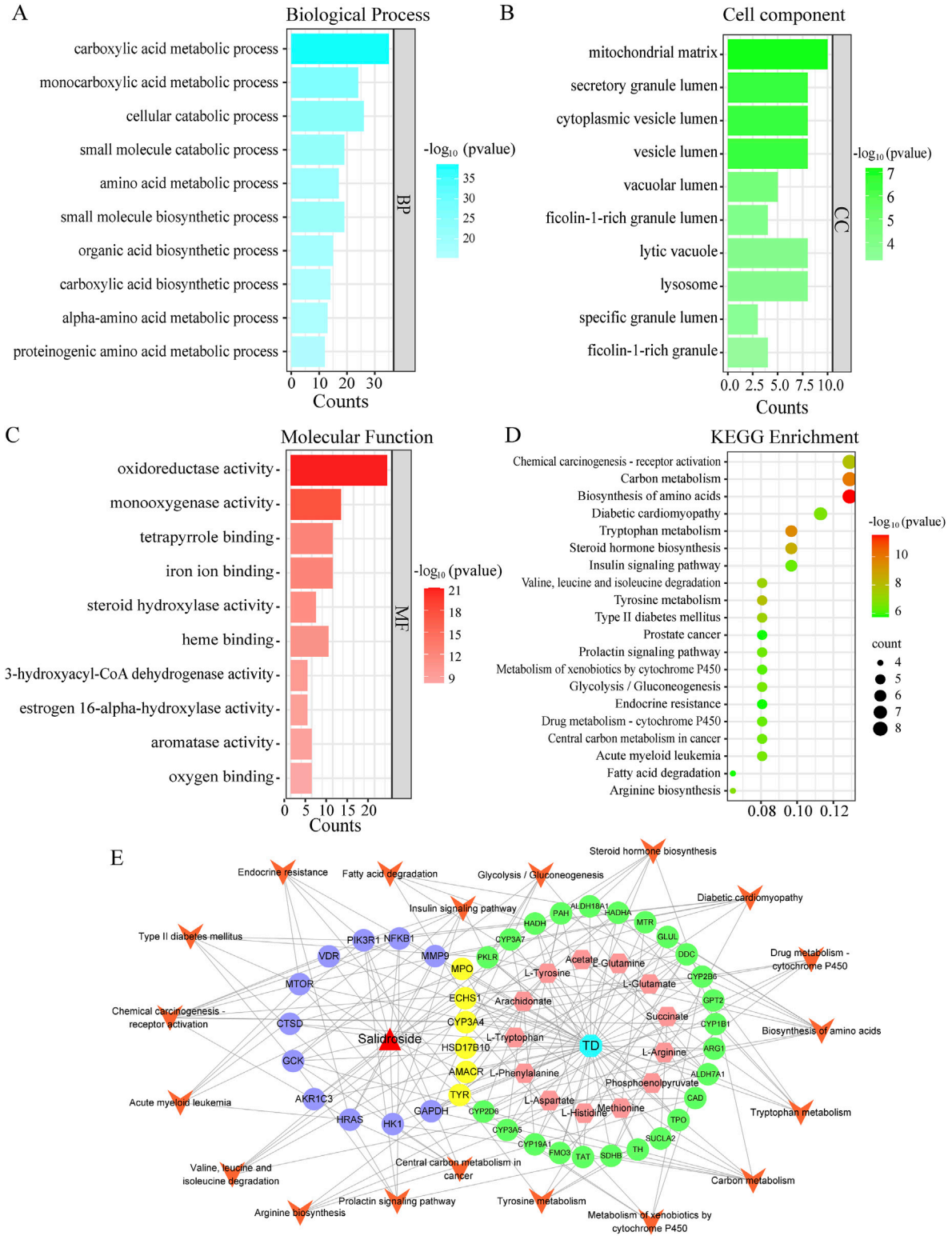

FIGURE 8
GO and KEGG analysis. **(A)** Biological process. **(B)** Cell component. **(C)** Molecular function. **(D)** Kegg enrichment. **(E)** "drug-metabolite-target-pathway-disease" network.

et al., 2024). Phenylalanine, classified as an essential aromatic amino acid, is metabolized by phenylalanine hydroxylase in bodily tissues, including the liver, ultimately leading to the production of dopamine (Wang et al., 2021). Dopamine plays a regulatory role in the hypothalamic-pituitary-gonadal axis, thereby supplying the requisite substrates for testosterone synthesis (Salonia et al.,

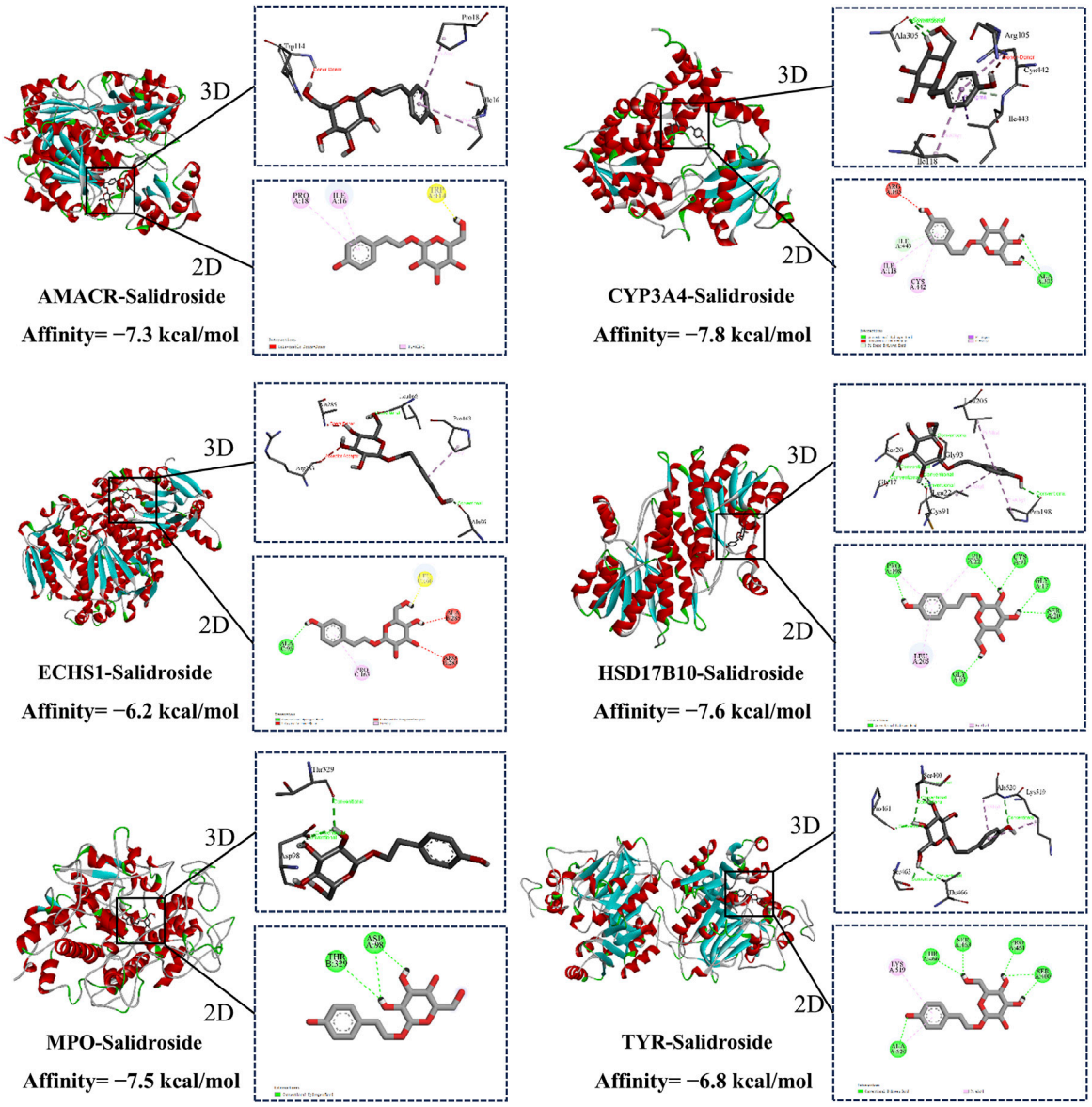

FIGURE 9
Molecular docking.

2019). In addition, pyruvate is the product of glycolytic pathway, which is located at the junction of anaerobic glycolysis and aerobic oxidation metabolism, and plays an important role in maintaining the metabolism of tissues and cells and ensuring energy (Liang et al., 2021).

To further investigate the mechanisms by which salidroside enhances testosterone secretion, this study employed an integrative approach combining metabolomics and network pharmacology. The research examined the correlation between upstream targets and downstream differential metabolites, culminating in the construction of a "drug-metabolite-target-pathway-disease" network. The findings indicated that the promotion of testosterone secretion by salidroside is closely associated with six key targets: AMACR, CYP3A4, ECHS1, HSD17B10, MPO, and TYR. It is noteworthy that CYP3A4, a cytochrome P450 enzyme, plays a crucial role in the metabolism of testosterone within the body, facilitating its conversion into metabolites such as 6β-hydroxytestosterone, which subsequently diminishes the biological activity of testosterone (Christiansen et al., 2011). Additionally, HSD17B10 (hydroxysteroid 17-β dehydrogenase 10) is a mitochondrial enzyme implicated in the metabolic processing of steroid hormones (He et al., 2023). During testosterone biosynthesis, HSD17B10 primarily catalyzes the conversion of androstenedione to testosterone. MPO is an enzyme present in neutrophils and eosinophils that plays a crucial role in mitigating oxidative damage and preserving cellular function (Michaeloudes et al., 2022). It serves to protect interstitial cells from oxidative stress and facilitates the secretion of testosterone. Furthermore, AMACR and ECHS1 are involved in the regulation of cholesterol metabolism, thereby influencing testosterone production (Hu et al., 2022; Mojanaga et al., 2024).

Subsequently, the impact of salidroside on the targets AMACR, CYP3A4, ECHS1, HSD17B10, MPO, and TYR was examined

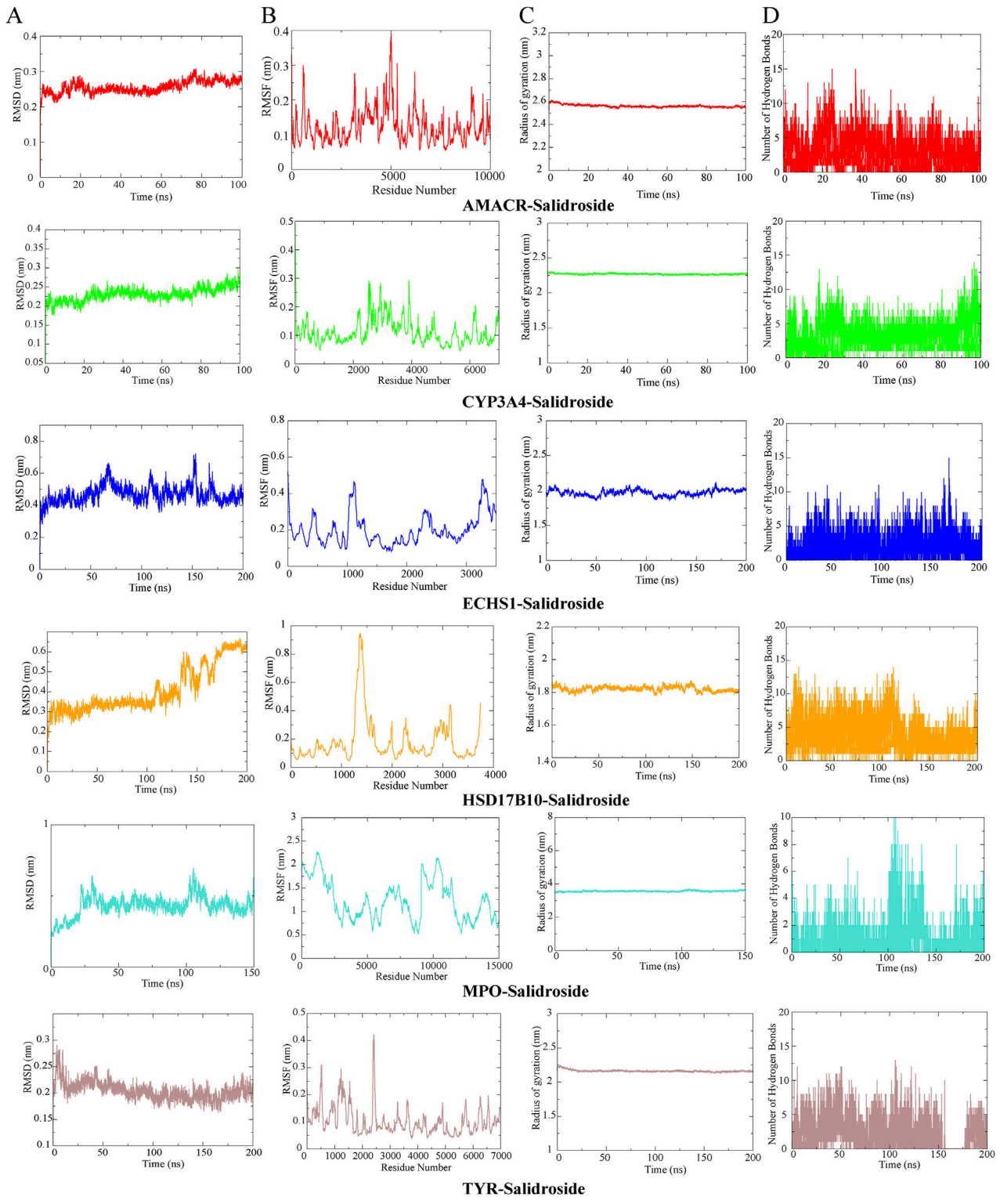

FIGURE 10
Molecular dynamics simulation. **(A)** RMSD analysis. **(B)** RMSF analysis. **(C)** RG analysis. **(D)** Hydrogen bond analysis.

through bioinformatics analysis and cellular experiments. Molecular docking studies revealed that the binding energy was lower than −5 kcal/mol, indicating a strong affinity, and its stability was confirmed via molecular dynamics simulations. Furthermore, RT-qPCR results demonstrated that salidroside significantly upregulated the expression levels of AMACR, ECHS1, HSD17B10, MPO, and TYR, while downregulating the expression of CYP3A4. It further strengthens the important position that salidroside may act on the above-mentioned core targets in promoting testosterone secretion.

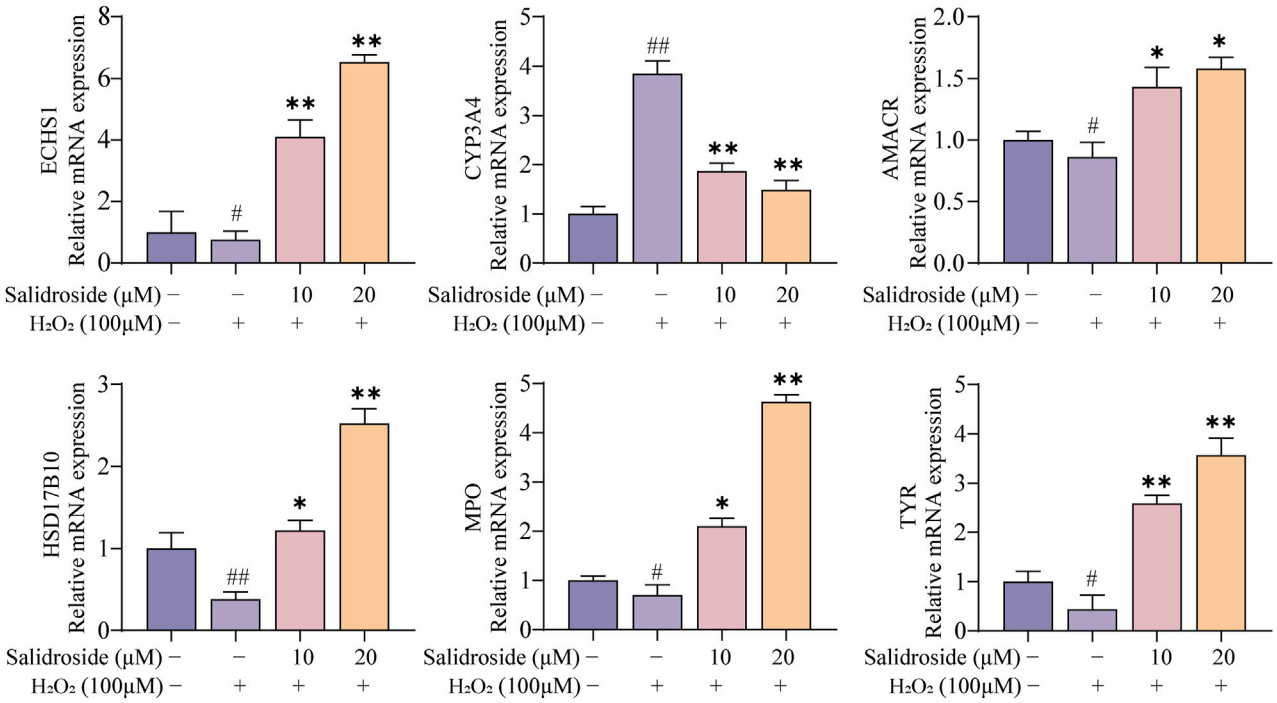

FIGURE 11
RT-qPCR analysis. (mean ± SD, n = 3). Compared with the control group, $^{\#}p < 0.05$, $^{\#\#}p < 0.01$; Compared with the model group, $^{*}p < 0.05$, $^{**}p < 0.01$.

5 Conclusion

In summary, this study utilized the TM3 cell model, induced by salidroside and H_2O_2, as the primary research focus. An integrative approach combining metabolomics and network pharmacology was employed to investigate the relationship between salidroside and the biological functions of the organism at a systemic level. The study analyzed the differential metabolites, core targets, and metabolic pathways associated with salidroside's promotion of testosterone secretion. However, it is worth noting that this study provides a preliminary theoretical and experimental basis for the study of the mechanism and clinical application of salidroside in promoting testosterone secretion, and also provides a new research idea and direction for the follow-up study of pharmacodynamic substances.

Data availability statement

The original contributions presented in the study are included in the article/supplementary material, further inquiries can be directed to the corresponding authors.

Ethics statement

Ethical approval was not required for the studies on animals in accordance with the local legislation and institutional requirements because only commercially available established cell lines were used.

Author contributions

ZW: Conceptualization, Formal Analysis, Investigation, Resources, Software, Writing–original draft. YX: Data curation, Methodology, Validation, Writing–review and editing. HX: Funding acquisition, Project administration, Supervision, Visualization, Writing–review and editing.

Funding

The author(s) declare that financial support was received for the research, authorship, and/or publication of this article. This work was financially supported by the Jilin Science and Technology Development Plan Project (No. YDZJ202301ZYTS184), National Famous Traditional Chinese Medicine Heritage Studio Project (Ji Traditional Chinese Medicine Fa [2022] No. 48).

Conflict of interest

The authors declare that the research was conducted in the absence of any commercial or financial relationships that could be construed as a potential conflict of interest.

Generative AI statement

The author(s) declare that no Generative AI was used in the creation of this manuscript.

Publisher's note

All claims expressed in this article are solely those of the authors and do not necessarily represent those of their affiliated organizations, or those of the publisher, the editors and the reviewers. Any product that may be evaluated in this article, or claim that may be made by its manufacturer, is not guaranteed or endorsed by the publisher.

Supplementary material

The Supplementary Material for this article can be found online at: https://www.frontiersin.org/articles/10.3389/fchem.2025.1544876/full#supplementary-material

References

Albuquerque, C. P., Freitas, F. R., Martinelli, A. E. M., Lima, J. H., Coelho, R. F., Serrano, C. V., Jr., et al. (2020). Androgen deprivation therapy improves the *in vitro* capacity of high-density lipoprotein (HDL) to receive cholesterol and other lipids in patients with prostate carcinoma. *Lipids Health Dis.* 19, 133. doi:10.1186/s12944-020-01305-8

Ashour, A. M. (2024). Propolis attenuates diabetes-induced testicular injury by protecting against DNA damage and suppressing cellular stress. *Front. Pharmacol.* 15, 1416238. doi:10.3389/fphar.2024.1416238

Aversa, A., and Morgentaler, A. (2015). The practical management of testosterone deficiency in men. *Nat. Rev. Urol.* 12, 641–650. doi:10.1038/nrurol.2015.238

Christiansen, A., Backensfeld, T., Denner, K., Weitschies, W. J. E. J. O. P., and Biopharmaceutics (2011). Effects of non-ionic surfactants on cytochrome P450-mediated metabolism *in vitro*. *Eur. J. Pharm. Biopharm.* 78, 166–172. doi:10.1016/j.ejpb.2010.12.033

Dalmasso, C., Patil, C. N., Yanes Cardozo, L. L., Romero, D. G., and Maranon, R. O. (2017). Cardiovascular and metabolic consequences of testosterone supplements in young and old male spontaneously hypertensive rats: implications for testosterone supplements in men. *J. Am. Heart Assoc.* 6, e007074. doi:10.1161/jaha.117.007074

Falvo, S., Santillo, A., Di Fiore, M. M., Venditti, M., Grillo, G., Latino, D., et al. (2024). New insights into D-aspartate signaling in testicular activity. *Cells* 13, 1400. doi:10.3390/cells13161400

Gao, Z., Zhan, H., Zong, W., Sun, M., Linghu, L., Wang, G., et al. (2023). Salidroside alleviates acetaminophen-induced hepatotoxicity via Sirt1-mediated activation of Akt/Nrf2 pathway and suppression of NF-κB/NLRP3 inflammasome axis. *Life Sci.* 327, 121793. doi:10.1016/j.lfs.2023.121793

Groti Antonič, K., and Zitzmann, M. (2024). Novel perspectives of testosterone therapy in men with functional hypogonadism: traversing the gaps of knowledge. *Aging Male* 27, 2296460. doi:10.1080/13685538.2023.2296460

He, X.-Y., Frackowiak, J., Dobkin, C., Brown, W. T., and Yang, S.-Y. J. I. J. O. M. S. (2023). Involvement of type 10 17β-hydroxysteroid dehydrogenase in the pathogenesis of infantile neurodegeneration and alzheimer's disease. *Int. J. Mol. Sci.* 24, 17604. doi:10.3390/ijms242417604

Hu, T., Chen, X., Lu, S., Zeng, H., Guo, L., Han, Y. J. T. I. C. R., and Treatment (2022). Biological role and mechanism of lipid metabolism reprogramming related gene ECHS1 in cancer. *Technol. Cancer Res. Treat.* 21, 15330338221140655. 15330338221140655-15330338221140655. doi:10.1177/15330338221140655

Li, M., Niu, Y., Zhang, T., Yang, H., Tian, L., Zhou, S., et al. (2024a). Wen-Shen-Tong-Luo-Zhi-Tong-Decoction inhibits bone loss in senile osteoporosis model mice by promoting testosterone production. *J. Ethnopharmacol.* 338, 119033. doi:10.1016/j.jep.2024.119033

Li, Z., Jia, B., Guo, Z., Zhang, K., Zhao, D., Li, Z., et al. (2024b). Therapeutic potential of salidroside in type I diabetic erectile dysfunction: attenuation of oxidative stress and apoptosis via the Nrf2/HO-1 pathway. *PLoS One* 19, e0306926. doi:10.1371/journal.pone.0306926

Liang, A., Huang, L., Liu, H., He, W., Lei, X., Li, M., et al. (2021). Resveratrol improves follicular development of PCOS rats by regulating the glycolytic pathway. *Mol. Nutr. Food Res.* 65, e2100457. doi:10.1002/mnfr.202100457

Lu, Y. S., Chen, J., He, X. R., Yang, S. L., Ma, B. J., Yu, J., et al. (2024). Perfluorooctane sulfonate (PFOS) and benzo[a]pyrene (BaP) synergistically induce neurotoxicity in C6 rat glioma cells via the activation of neurotransmitter and Cyp1a1-mediated steroid hormone synthesis pathways. *Food Chem. Toxicol.* 193, 115058. doi:10.1016/j.fct.2024.115058

Maniscalco, M., Cutignano, A., Paris, D., Melck, D. J., Molino, A., Fuschillo, S., et al. (2020). Metabolomics of exhaled breath condensate by nuclear magnetic resonance spectroscopy and mass spectrometry: a methodological approach. *Curr. Med. Chem.* 27, 2381–2399. doi:10.2174/0929867325666181008122749

Mbiydzenyuy, N. E., and Qulu, L.-a.J. M. B. D. (2024). Stress, hypothalamic-pituitary-adrenal axis, hypothalamic-pituitary-gonadal axis, and aggression. *Metab. Brain Dis.* 39, 1613–1636. doi:10.1007/s11011-024-01393-w

Michaeloudes, C., Abubakar-Waziri, H., Lakhdar, R., Raby, K., Dixey, P., Adcock, I. M., et al. (2022). Molecular mechanisms of oxidative stress in asthma. *Mol. Asp. Med.* 85, 101026. doi:10.1016/j.mam.2021.101026

Mojanaga, O. O., Woodman, T. J., Lloyd, M. D., and Acharya, K. R. (2024). α-Methylacyl-CoA racemase from Mycobacterium tuberculosis-detailed kinetic and structural characterization of the active site. *Biomolecules* 14, 299. doi:10.3390/biom14030299

Nassar, G. N., and Leslie, S. W. (2023). *Physiology, testosterone*. Treasure Island (FL): StatPearls Publishing.

Pognan, F., Beilmann, M., Boonen, H., Czich, A., Dear, G., Hewitt, P., et al. (2023). The evolving role of investigative toxicology in the pharmaceutical industry. *Nat. Rev. Drug Discov.* 22, 317–335. doi:10.1038/s41573-022-00633-x

Rasmussen, R. S., Midttun, M., Zerahn, B., Pedersen, M., Rashid, A., Østergren, P. B., et al. (2024). Testosterone and resistance training improved physical performance and reduced fatigue in frail older men: 1 year follow-up of a randomized clinical trial. *Aging Male* 27, 2403519. doi:10.1080/13685538.2024.2403519

Roshanzamir, F., and Safavi, S. M. (2017). The putative effects of D-Aspartic acid on blood testosterone levels: a systematic review. *Int. J. Reprod. Biomed.* 15, 1–10. doi:10.29252/ijrm.15.1.1

Salonia, A., Rastrelli, G., Hackett, G., Seminara, S. B., Huhtaniemi, I. T., Rey, R. A., et al. (2019). Paediatric and adult-onset male hypogonadism. *Nat. Rev. Dis. Prim.* 5, 38. doi:10.1038/s41572-019-0087-y

Schenck, C. A., and Maeda, H. a.J. P. (2018). Tyrosine biosynthesis, metabolism, and catabolism in plants. *Phytochemistry* 149, 82–102. doi:10.1016/j.phytochem.2018.02.003

Tsuchiya, H., Fujinoki, M., Azuma, M., and Koshimizu, T. A. (2023). Vasopressin V1a receptor and oxytocin receptor regulate murine sperm motility differently. *Life Sci. Alliance* 6, e202201488. doi:10.26508/lsa.202201488

Wang, Y., Tong, Q., Ma, S. R., Zhao, Z. X., Pan, L. B., Cong, L., et al. (2021). Oral berberine improves brain dopa/dopamine levels to ameliorate Parkinson's disease by regulating gut microbiota. *Signal Transduct. Target Ther.* 6, 77. doi:10.1038/s41392-020-00456-5

Wishart, D. S. J. P. R. (2019). Metabolomics for investigating physiological and pathophysiological processes. *Physiol. Rev.* 99, 1819–1875. doi:10.1152/physrev.00035.2018

Wu, G., Meininger, C. J., Mcneal, C. J., Bazer, F. W., and Rhoads, J. M. (2021). Role of L-arginine in nitric oxide synthesis and health in humans. *Adv. Exp. Med. Biol.* 1332, 167–187. doi:10.1007/978-3-030-74180-8_10

Wu, Z., Ma, Y., Chen, S., Liu, Y., Liu, X., Cao, H., et al. (2024). Arginine biosynthesis mediates wulingzhi extract resistance to busulfan-induced male reproductive toxicity. *Int. J. Mol. Sci.* 25, 6320. doi:10.3390/ijms25126320

Ye, M., Zhao, F., Ma, K., Zhou, K., Ma, J., Fu, H., et al. (2021). Enhanced effects of salidroside on erectile function and corpora cavernosa autophagy in a cavernous nerve injury rat model. *Andrologia* 53, e14044. doi:10.1111/and.14044

Zhang, J., Fang, Y., Tang, D., Xu, X., Zhu, X., Wu, S., et al. (2022). Activation of MT1/MT2 to protect testes and Leydig cells against cisplatin-induced oxidative stress through the SIRT1/nrf2 signaling pathway. *Cells* 11, 1690. doi:10.3390/cells11101690

Zhang, X. D., Sun, J., Zheng, X. M., Zhang, J., Tan, L. L., Fan, L. L., et al. (2024). Plin4 exacerbates cadmium-decreased testosterone level via inducing ferroptosis in testicular Leydig cells. *Redox Biol.* 76, 103312. doi:10.1016/j.redox.2024.103312

Zhu, M., and Yu, J. (2024). Salidroside alleviates ferroptosis in FAC-induced Age-related macular degeneration models by activating Nrf2/SLC7A11/GPX4 axis. *Int. Immunopharmacol.* 142, 113041. doi:10.1016/j.intimp.2024.113041